A TRADE STUDY OF BIOHYBRID MICROROBOTS: COMPARING ACTUATION AND LOCALIZATION OF IRONSPERM

Bachelor Thesis of Mohan Bloxs

Department of Biomechanical Engineering – Faculty of Engineering Technology

EXAMINATION COMMITTEE

Dr. Islam S. M. Khalil

Prof. Dr. Sarthak Misra

Dr. Janset Dasdemir

ET-BT report number: BE-937

27– 06 – 2023

UNIVERSITY OF TWENTE.

Abstract

In recent years, untethered biohybrid microrobots have shown great promise for in vitro magnetic actuation and localization using medical imaging techniques. One type of untethered biohybrid microrobots is IRONSperm cells, which consist of dead bovine sperm cells coated with Iron Oxide nanoparticles that allow for magnetic actuation and enhance localization using ultrasound imaging. When increasing the Iron Oxide concentration, a trade-off occurs between the magnetic actuation, ultrasound localization, and the biocompatibility of IRONSperm clusters. To date, it was unknown how an increase in Iron Oxide concentration affected this trade-off. The aim of this study is to investigate the influence of an increasing concentration of Iron Oxide nanoparticles on the actuation and localization of IRONSperm clusters. This influence is determined by actuating different IRONSperm samples at increasing frequencies and imaging them with ultrasound. For the actuation, the average angular velocity of the different samples will be determined and for the localization, the ultrasound contrast-to-noise ratio will be determined. It is found that the angular velocity and contrast to noise ratio increase with increasing Iron Oxide concentration but because the cluster size of the different samples also differed, it cannot be concluded that the increase in angular velocity and contrast to noise ratio depend solely on the Iron Oxide concentration increase. Investigating the influence of Iron Oxide concentration will help to determine the optimal consistency of IRONSperm clusters for future research toward *in vivo* applications.

Table of Content

A TRADE STUDY OF BIOHYBRID MICROROBOTS: COMPARING ACTUATION AND LOCALIZATION OF IRONSPERM

Mohan Bloxs

***Abstract*— In recent years, untethered biohybrid microrobots have shown great promise for in vitro magnetic actuation and localization using medical imaging techniques. One type of untethered biohybrid microrobots is IRONSperm cells, which consist of dead bovine sperm cells coated with Iron Oxide nanoparticles that allow for magnetic actuation and enhance localization using ultrasound imaging. When increasing the Iron Oxide concentration, a trade-off occurs between the magnetic actuation, ultrasound localization, and the biocompatibility of IRONSperm clusters. To date, it was unknown how an increase in Iron Oxide concentration affected this trade-off. The aim of this study is to investigate the influence of an increasing concentration of Iron Oxide nanoparticles on the actuation and localization of IRONSperm clusters. This influence is determined by actuating different IRONSperm samples at increasing frequencies and imaging them with ultrasound. For the actuation, the average angular velocity of the different samples will be determined and for the localization, the ultrasound contrast-to-noise ratio will be determined. It is found that the angular velocity and contrast to noise ratio increase with increasing Iron Oxide concentration but because the cluster size of the different samples also differed, it cannot be concluded that the increase in angular velocity and contrast to noise ratio depend solely on the Iron Oxide concentration increase. Investigating the influence of Iron Oxide concentration will help to determine the optimal consistency of IRONSperm clusters for future research toward *in vivo* applications.**

I. INTRODUCTION

In recent years the development of biohybrid microrobots has shown significant promise for different biomedical applications like *in vitro* drug delivery [1]–[4] or fertilization [5], [6]. These biohybrid microrobots consist of biological cells and artificial components [1]–[12]. Combining the advantages of biological cells shaped by thousands of years of evolution, together with state-of-the-art technologies, researchers hope to overcome the barriers that arise in many biomedical applications. Several key advantages of these microrobots are remote actuation and biocompatibility [1]–[12]. However, since these microrobots have the potential to be used *in vivo* they not only need to be remotely actuated but also localized by an imaging modality. Several imaging modalities that have already been used to image microrobots are for example MRI [7], fluoroscopy [5], [7] and ultrasound [3], [4], [9], [10]. Even though all of these imaging modalities have their advantages and limitations, in this paper the focus is on ultrasound because it is radiation-free, allows for real-time imaging, and is both low in cost and clinically easily applicable.

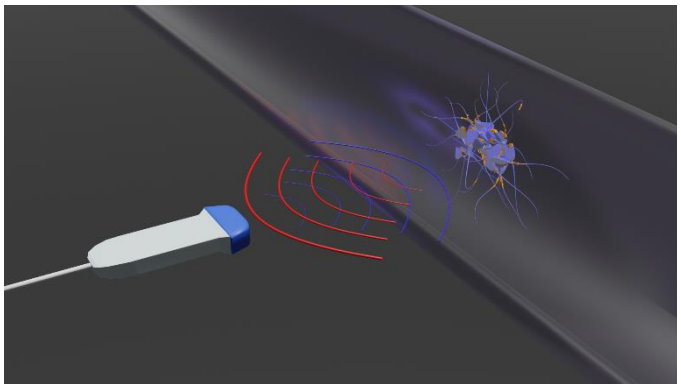

Figure 1 Graphical representation of a cluster of IRONSperm cells coated with Iron Oxide nanoparticles, imaged with ultrasound.

To ensure that the microrobots are biocompatible, can be actuated by magnetic fields, and can be imaged with ultrasound, the combination of biological cells and artificial component must be incorporated to provide a unique response not possible using the organic body. In recent studies the use of sperm cells coated with magnetic particles (Figure 1) has proven to be a suitable combination, which is mainly due to the intrinsic flexibility of the sperm cells while the coating of magnetic particles allows for magnetic actuation and increases the acoustic impedance of the sperm cells [3]–[6], [11], [12]. The use of magnetic particles negatively influences the biocompatibility, however [2]–[4], [7]. This means that a trade-off between the actuation, localization, and biocompatibility occurs where the actuation and localization are positively affected, while the biocompatibility is negatively affected.

Despite recent advances, there are still significant hurdles to overcome for the actuation, localization, and biocompatibility of such coated sperm cells. Ultrasound is a promising method for localizing clusters of coated sperm cells, however, because of the limited resolution and contrast-to-noise ratio (CNR) of ultrasound imaging, it is almost impossible to image individually coated sperm cells [3]–[6]. Furthermore, the magnetic actuation of individually coated sperm cells is only possible at low Reynolds numbers because the velocity is limited by the maximum generated propulsive thrust [4], [11].

Rather than focusing on individual microrobots, several studies have focused on actuating swarms or clusters of

microrobots [1], [7], [8]. In the case of sperm coated-microrobots, Middelhoek *et al.* have shown that it is also possible to actuate clusters of coated sperm cells [3]. In their experiment, they used Iron Oxide (Fe_3O_4) nanoparticles electrostatically assembled around dead bovine sperm cells, which they refer to as IRONSperm. These IRONSperm clusters, when actuated, will perform a rolling locomotion over a surface and it has been shown that this rolling speed is fifty times faster than the swimming velocity of individually coated sperm cells. Besides the higher achievable velocities, using clusters of coated sperm cells, rather than individual ones, also yields a higher detectable ultrasound signal and improves loading capacity due to the higher volumes of available sperm cells and nanoparticles [1], [7], [8].

Because of the trade-off that occurs, it is still unknown what consistency of sperm cells and magnetic nanoparticles can best be used to optimize the actuation and localization. This trade-off is dependent on the concentration of Fe_3O_4 nanoparticles. It is expected that when increasing the concentration of nanoparticles, both the actuation and localization of the microrobots will improve.

This study aims to determine the optimal concentration of Iron Oxide nanoparticles attached to the IRONSperm cells in order to optimize both the magnetic actuation and ultrasound localization. For the actuation, we will first predict the magnetic torque exerted on a cluster of IRONSperm for varying Fe_3O_4 concentration. After this we will experimentally determine the angular velocity of different clusters of IRONSperm with increasing concentration of Fe_3O_4, rolling through an actuation tube with an inner diameter of 1,1cm and filled with water. The cluster will perform a rolling locomotion when it is close to a surface and under the influence of a rotating permanent magnet (RPM). For the localization, we will determine the average CNR of an ultrasound video that captures the cluster rolling. The different samples that are used are shown in Table I and the setup used for actuation is shown in Figure 2.

Table I

Consistency of different IRONSperm samples used. V_S and V_N are the volumes of the Suspension and Nanoparticles respectively. C_C and C_N are the concentrations of sperm cells and nanoparticles respectively.

Sample	V_S (µl)	C_C (cells/ml)	V_N (µl)	C_N (mg/ml)
1	500	6.375×10^7	0	0
2	550	7.013×10^7	50	1
3	600	7.650×10^7	100	2
4	650	8.288×10^7	150	3

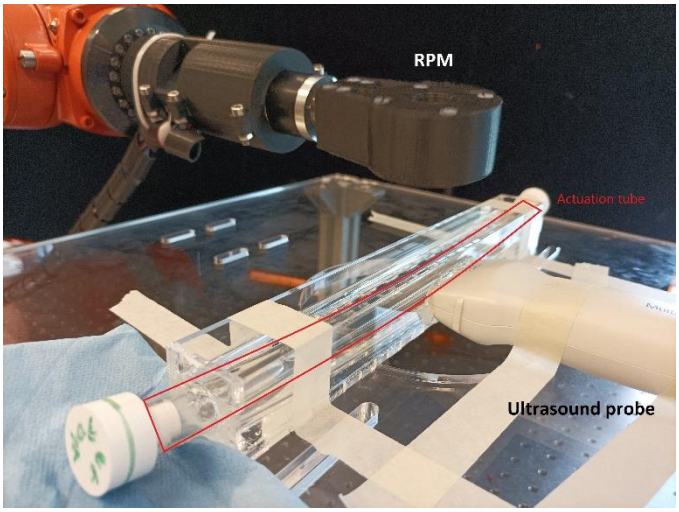

Figure 2 Experimental setup used for actuating the samples showing the RPM, ultrasound probe, and the container filled with water in which the actuation tube is placed. The actuation tube is also filled with water through which the clusters move.

II. Magnetic Torque Prediction and Angular Velocity Determination

IRONSperm are made by self-assembly of negatively charged, dead bovine sperm cells and positively charged Iron Oxide nanoparticles. This is made possible due to the electrostatic forces that occur between the two components. These coated IRONSperm aggregate into clusters because of physical interactions like Van der Waal forces and magnetic attractions. However, because the division and concentration of nanoparticles attached to the surface of sperm cells are dependent on the surface charge of these sperm cells, and since this surface charge differs between individual sperm cells, the sperm cells will differ individually. This also means that clusters of IRONSperm are likely made up of heterogeneous samples of IRONSperm. Because of its heterogeneity, the electrostatic and magnetic interactions between different clusters of IRONSperm also differ. This will, in turn, affect the magnetic response to the externally applied magnetic field. Besides the formation of IRONSperm due to self-assembly it has also been shown that clusters of IRONSperm maintain a stable configuration after the external magnetic field has been removed. Furthermore, by changing the concentration of nanoparticles and sperm cells, the magnetic field strength applied during self-assembly, or the self-assembly time, the cluster size can be varied [3], [4], [12], [13].

When an external magnetic field is applied on a cluster of IRONSperm, close to a surface and in a low Reynolds number environment, so that inertia is negligible, the magnetic moment of the cluster will try to align with the direction of the applied magnetic field resulting in a rolling movement. During rolling, the cluster tends to take an ellipsoidal shape as shown in Figure 4(A-C).

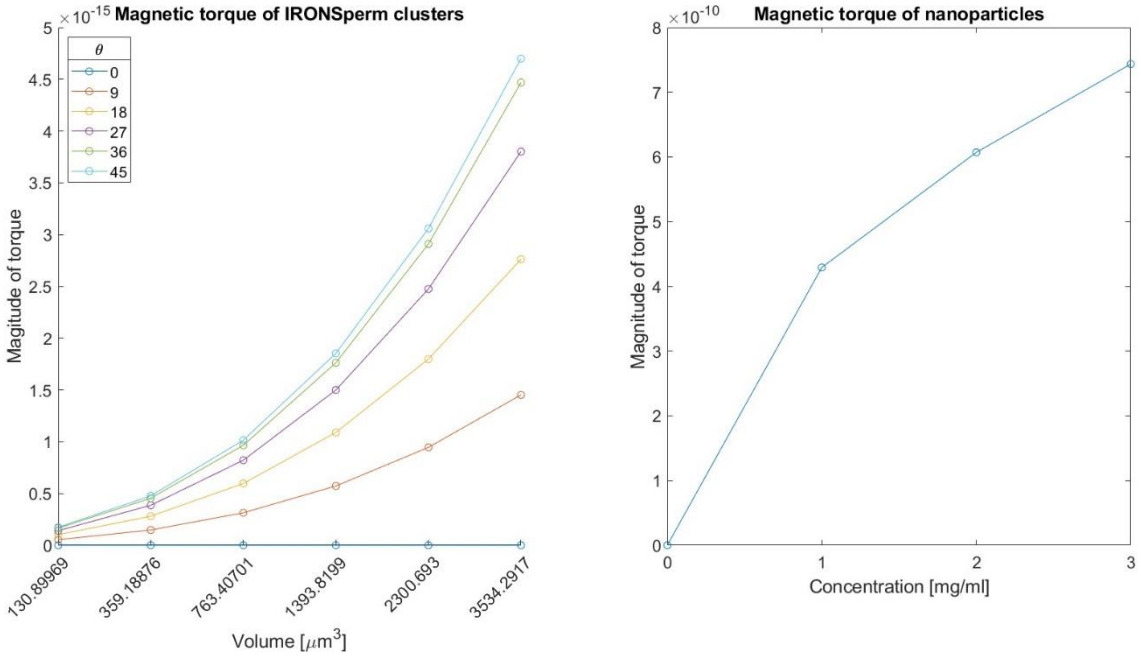

Figure 3 (Left) Predicted magnetic torque of an IRONSperm cluster for increasing cluster size and different orientations. (Right) Predicted magnetic torque of an IRONSperm cluster with increasing concentration of Fe_3O_4 (Right).

Furthermore, because the Fe_3O_4 nanoparticles are ferromagnetic, the cluster will be approximated as a soft magnetic, ellipsoidal body. When the applied magnetic field strength is sufficiently low such that $|\mathbf{m}| < m_s$, where m_s is the saturation magnetization of an IRONSperm cluster, the magnitude of the magnetic torque is given by [14]:

$$|\boldsymbol{\tau}_\mathrm{m}| = \frac{\mu_0 V |n_r - n_a|}{2 n_a n_r} |\mathbf{H}|^2 \sin(2\theta), \qquad (1)$$

where μ_0 is the permeability of free space, V is the volume of the IRONSperm cluster, n_r and n_a are the demagnetization factors in the long and short axis of the ellipsoid respectively, $\mathbf{H}$ is the magnitude of the applied magnetic field and θ is the angle between the axis of symmetry of the cluster and the direction of the external magnetic field. It follows that the magnetic torque is maximized when $\theta = 45°$. From Equation (1) it follows that the expected magnitude of the magnetic torque depends on the volume of the cluster and its orientation when a uniform magnetic field is applied. Equation (1) is determined for clusters with a volume of 130μm up to 3500μm. For every volume, it is assumed that the ratio of the long and short axis of the cluster equals 2 and that all clusters thus have a similar shape. The results are calculated with a MATLAB script (Appendix A) and are shown in Figure 3. It can be seen that for an increasing cluster volume and orientation, the magnitude of the magnetic torque increases.

The speed of locomotion of a cluster depends on the frequency with which the RPM rotates. Clusters of IRONSperm have a certain step-out frequency and if they are actuated above this frequency, the cluster will undergo oscillations that are superimposed on the rotational motion, thus decreasing its angular velocity. Furthermore, due to the superimposed oscillations, large clusters of IRONSperm may start to lag or break apart, forming smaller clusters of IRONSperm. When clusters are actuated below this step-out frequency, however, it has been found that the angular velocity of the clusters is equal to the frequency of the RPM [3], [15]. Because of the decreased angular velocity when actuated above the step-out frequency, and the fact that larger clusters may break apart into smaller clusters, which likely decreases both the detectability of IRONSperm clusters and their CNR, as well as their drug loading capabilities, this research will only focus on clusters of IRONSperm that are actuated below the step-out frequency. The step-out frequency of IRONSperm clusters is, however, dependent on the magnetic moment exerted on them and their drag coefficient [3], [15]. Therefore the step-out frequency differs per IRONSperm cluster and first needs to be determined. This can be done by actuating clusters of IRONSperm at increasing frequencies until the cluster no longer rolls uniformly over the surface, but rather starts lagging or rotating around its axis.

As mentioned before, the concentration of Fe_3O_4 Nanoparticles can be varied to gain different samples of IRONSperm. Carrey *et al.* have shown that, when changing the concentration of Magnetic NanoParticles (MNP) in a certain assembly, an increase in MNP concentration results in a higher magnetic torque exerted on the total assembly. They conducted these experiments under the influence of magnetic fields in the range of 10-50 mT with MNP's whose anisotropy differed per nanoparticle. These conditions are similar to the ones that are used in this research to actuate IRONSperm clusters. Because of this, it is expected that, when increasing the concentration of Fe_3O_4 in IRONSperm samples, the total magnetic torque exerted on an IRONSperm cluster will also increase. The total magnetic torque exerted on a cluster of IRONSperm with increasing concentration of Fe_3O_4 can then be approximated by [16]:

$$\boldsymbol{\tau}_\mathrm{t} = \boldsymbol{\tau}_1 \sqrt{n}, \qquad (2)$$

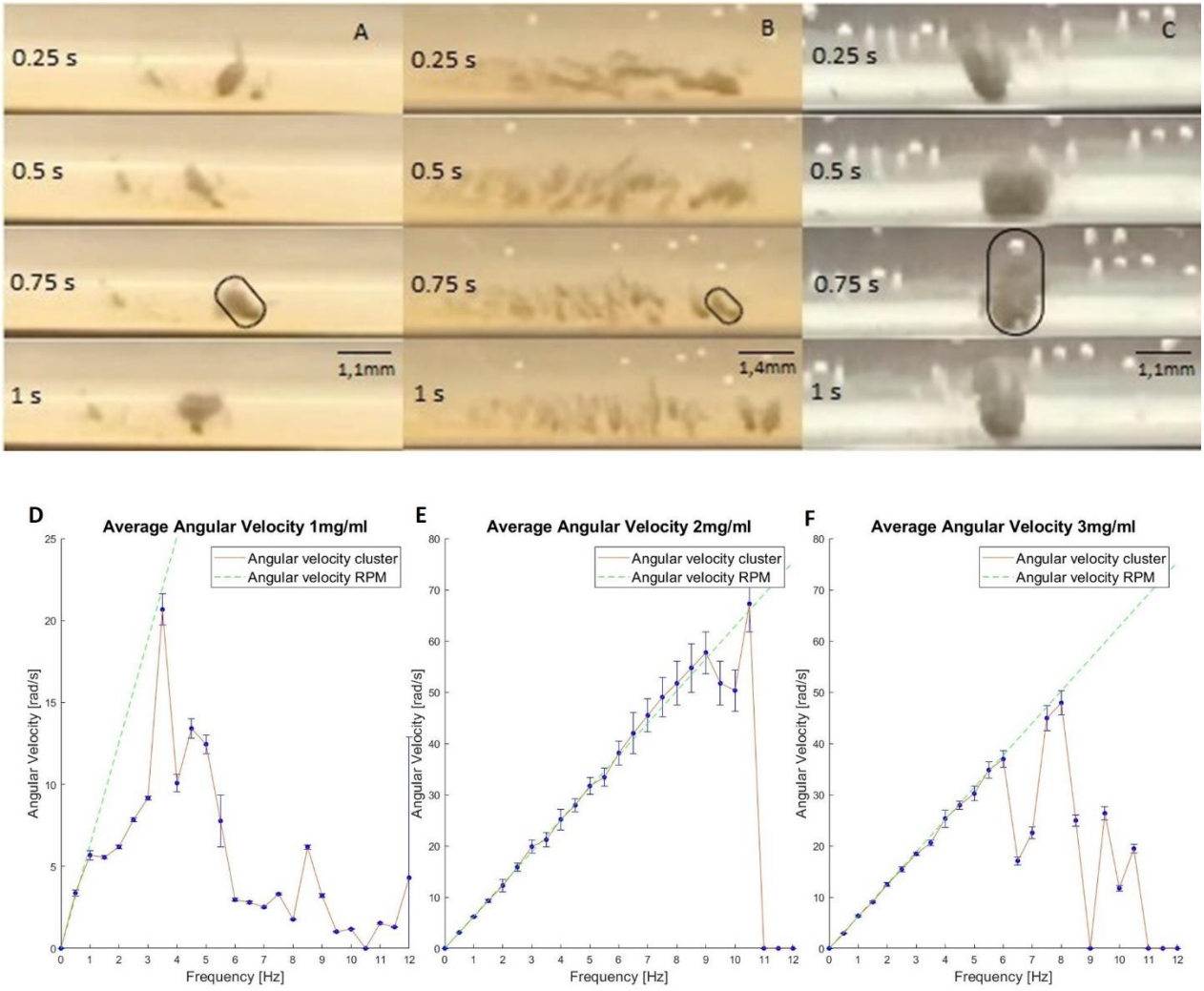

Figure 4 As clusters of IRONSperm are actuated by the RPM they perform a rolling locomotion over the surface of the PVC tube. In this case, the clusters are actuated to the right. (A-C) Samples 2-4 are actuated by the RPM at a frequency of 1.5Hz. The respective cluster diameters are 1.41mm, 1.2mm, and 2.83mm based on the prolate ellipses drawn over the clusters. (D-F) The average angular velocities of samples 2-4 as they are actuated at frequencies from 0.5-12Hz compared to the angular velocity of the RPM. The respective step-out frequencies of samples 2 and 4 are 3.5 and 6Hz. For sample 3 no step-out frequency could be determined.

where n is the total amount of Fe_3O_4 nanoparticles attached to the IRONSperm cells and τ_1 is the magnetic torque exerted on one Fe_3O_4 nanoparticle. The magnetic torque on one Fe_3O_4 nanoparticle can be calculated by [16]:

$$\boldsymbol{\tau_1} = \boldsymbol{\tau_{max}} \sqrt{1 - \left(\frac{\mu_0 M \mathbf{H}}{2K_{eff}}\right)^2}, \qquad (3)$$

where M is the magnetization per unit volume, K_{eff} is the uniaxial anisotropy and $\boldsymbol{\tau_{max}}$ is the maximum magnetic torque that one Fe_3O_4 particle can undergo. $\boldsymbol{\tau_{max}}$ can be calculated by: $\boldsymbol{\tau_{max}} = \mu_0 M V_n \mathbf{H}$, where V_n is the volume of a Fe_3O_4 nanoparticle. The results of Equation (2) are calculated with a MATLAB script (Appendix A) and are plotted in Figure 3. Because the volume increase linearly with the concentration, the magnetic torque can be plotted against the concentration of the different samples. It can be seen that for an increased Fe_3O_4 concentration, the magnitude of the magnetic torque on the nanoparticles also increases.

In order to experimentally determine the influence of increasing cluster volume and Fe_3O_4 concentration on the magnetic torque of an IRONSperm cluster, the average angular velocity of the different samples of IRONSperm will be calculated. Because the magnetic torque causes an IRONSperm cluster to roll, the angular velocity will be proportional to the magnetic torque. The average angular velocity of the different IRONSperm samples is calculated with a MATLAB script (Appendix B). For this, the number of complete rotations was counted and the total angular change was divided by the time. The results are plotted in Figure 4. In Figure 4(A-C) the rolling motion of samples 2-4 is shown at different time intervals. Sample 1 does not contain any Fe_3O_4 and therefore does not respond to any magnetic field. Sample 1 therefore also does not have an angular velocity. Furthermore, it can be seen that samples 2 and 4 form large clusters and maintain this configuration while rolling. Sample 3 however, does not form into a large cluster, but instead forms many smaller clusters. The cluster diameter of samples 2-4 are 1.41mm, 1.2mm, and 2.83mm respectively. These diameters were determined based on the ellipses drawn in Figure 4(A-C).

For samples 2 and 4 the step-out frequency is 3.5Hz and 6Hz respectively. At higher frequencies, the clusters start to lag during their rolling locomotion and their rolling is no longer uniform. Figure 4(D) shows that the average angular velocity of sample 2 reaches its peak angular velocity at 3.5Hz. After 3.5Hz the velocity decreases again but there is still an increasing trend for frequencies 4 and 4.5Hz. At these frequencies, the cluster no longer rolls uniformly, however. Instead, the cluster starts lagging or rotating quickly around its axis. The peak angular velocity is determined to be the angular velocity at the step-out frequency of 3.5Hz, which is 20,67 rad/s.

For sample 4 it can be seen in Figure 4(F) that the average angular velocity increases up to 6Hz but that it significantly drops for frequencies 6.5 and 7Hz. For frequencies 6.5 and 7Hz, the cluster no longer rolls uniformly and starts to lag. This can also be seen in Figure 4(F), where there is a significant decrease in angular velocity for these frequencies. The cluster rolls uniformly again, however, for frequencies 7.5 and 8Hz, which is also backed by an increase in angular velocity in Figure 4(F). Because the cluster starts to lag at 6.5Hz however, the step-out frequency of sample 3 is determined to be 6Hz. The corresponding average angular velocity at 6Hz is 36.93 rad/s.

As shown in Figure 4(B), sample 3 does not form one big cluster but rather multiple small ones. In Figure 4(E) it can be seen that the average angular velocity increases up to 10.5Hz, after which the clusters rotated so fast that it was impossible to determine the angular velocity with the used equipment. At 10.5Hz the average angular velocity is 67.25 rad/s. At 10.5Hz the clusters did perform a uniform rolling even at high frequencies and achieved much higher angular velocities than samples 2 and 4. These clusters were however much smaller than the clusters used in samples 2 and 4.

Another way to define the step-out frequency would be to compare the calculated average angular velocity with the angular velocity of the RPM. As mentioned before, when clusters of IRONSperm are actuated below the step-out frequency, the angular velocity of the clusters should equal the angular velocity of the RPM. In Figure 4(D-F) it can be seen that the angular velocity of samples 2 and 4 nearly coincides with the angular velocity of the RPM at the determined step-out frequencies of 3.5 and 6Hz. Sample 3 coincides with the angular velocity of the RPM over all frequencies up to 10Hz.

III. Localization using ultrasound imaging

For *in vitro* experiments, it suffices to use optical imaging modalities like a camera to follow the moving IRONSperm clusters but for *in vivo* experiments this is no longer possible since you will not be able to see the clusters anymore. Because of this, it is necessary to use a medical imaging modality instead. In this case, ultrasound will be used because it is radiation-free and allows for real-time imaging.

When ultrasound waves are transmitted through a medium, they will partly reflect when they encounter other media with different acoustic impedances. The velocity, c, with which the waves travel through the medium, is dependent on the density of the medium. This velocity corresponds with the speed of sound and is typically 1540 m s^{-1} and 1500 m s^{-1} for tissue and water respectively. When the acoustic impedance mismatch is bigger between different media, the reflection coefficient is also bigger and a bigger portion of the incoming wave is reflected. Because of the acoustic impedance mismatch between the bovine sperm cells and Fe_3O_4 nanoparticles in IRONSperm clusters, they can thus be detected with ultrasound. There is however a limitation to the maximum size of IRONSperm clusters that can be detected. The axial resolution of ultrasound is equal to the wavelength, λ, of the ultrasound waves, which can be given by $\lambda = \frac{c}{f}$, where f is the frequency of the ultrasound waves. This means that for an ultrasound transducer that emits waves with a frequency of 14 MHz in water, IRONSperm clusters with a diameter of 100μm can be detected [3], [4].

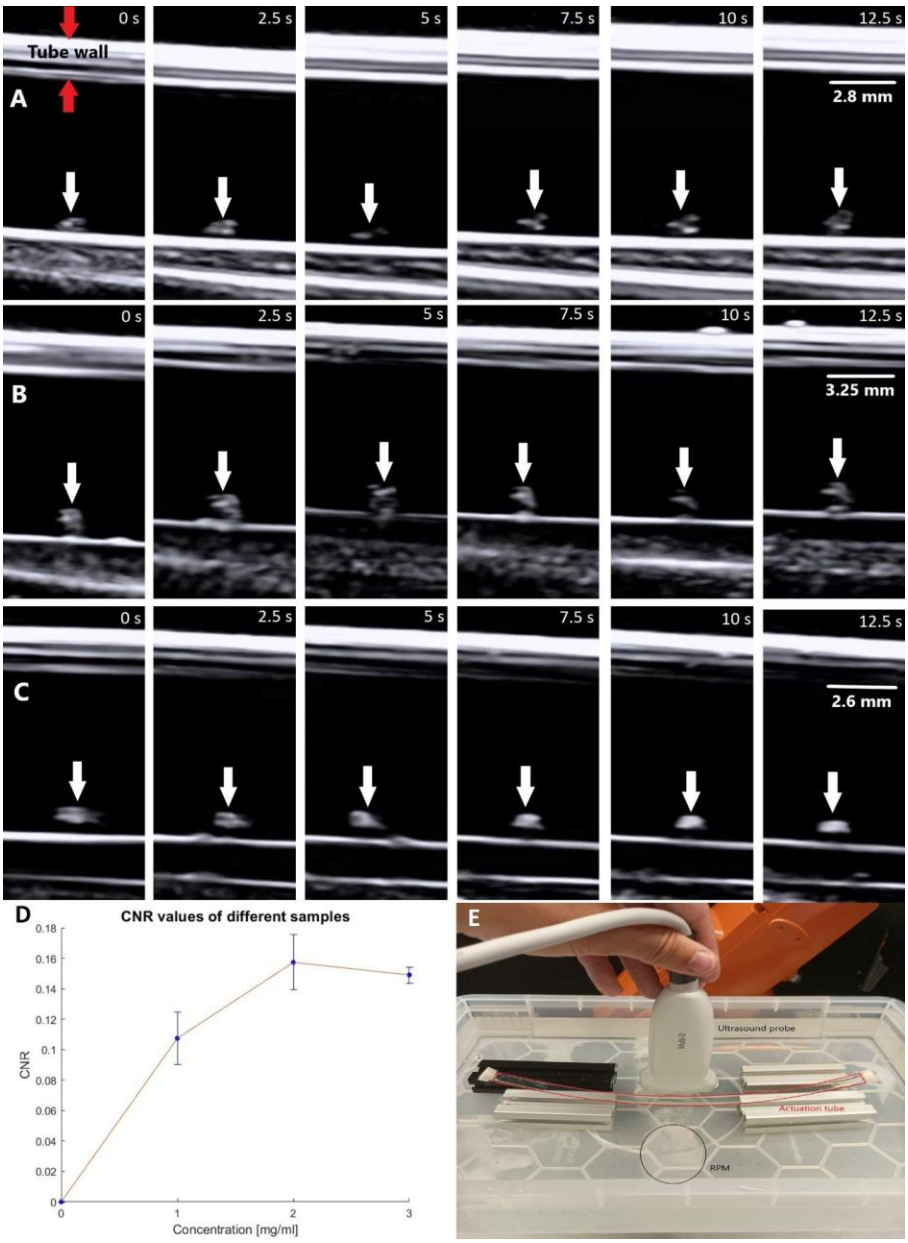

Figure 5 Ultrasound images of different IRONSperm samples while they were actuated. (A-C) Ultrasound images of samples 2-4 while being actuated at 0.5Hz with 14MHz ultrasound waves at a depth of approximately 1.5cm. The white arrows represent the clusters. The respective cluster diameters are 1.18mm, 1.5mm, and 1.2mm. (D) Calculated CNR values of all samples with error bars. (E) Used setup for localizing the IRONSperm clusters.

Increasing the concentration of Fe_3O_4 nanoparticles attached to the surface of IRONSperm cells will not only influence the actuation of IRONSperm clusters, but it will also influence the localization of IRONSperm clusters. Yang *et al.* have shown that when increasing the concentration of SuperParamagnetic Iron Oxide (SPIO) nanoparticles in Encapsulated MicroBubbles (EMBs), often used as contrast agent for MRI or US, the image brightness also increased in the regions where these EMBs were added [17]. They did so by calculating a 'mean grey scale' for a certain Region Of Interest (ROI). They did however find that this increase in brightness occurred up till a certain concentration of SPIO nanoparticles. After this concentration was reached, the mean grey scale decreased again. Because of this, it is expected that, when increasing the concentration of Fe_3O_4 nanoparticles at the surface of IRONSperm cells, the brightness of the US images will also increase at the place of the IRONSperm clusters. This increase is, however also expected to occur only up to a certain concentration of Fe_3O_4 nanoparticles.

To determine the CNR, rather than the image brightness, a MATLAB script (Appendix C) has been made. In this script, a self-selected Region Of Interest (ROI), which corresponds to an IRONSperm cluster, was determined. A second region was determined in the noisy background of the image. The mean

grayscale was then determined of this ROI, as well as of the background. The *CNR* can then be calculated by [18]:

$$CNR = \frac{|S_A - S_B|}{\sigma_B}, \quad (4)$$

where S_A and S_B are the mean grey scales of the ROI and the background respectively and σ_B is the standard deviation of the region in the background. Since it is expected that the image brightness of the IRONSperm clusters will increase with increasing concentration of Fe_3O_4 concentrations, it is also expected that the CNR will also increase. This is because an increase in Fe_3O_4 concentration will only affect S_A and not the background.

In order to localize the IRONSperm clusters using ultrasound, a new setup was used, shown in Figure 5(E). The setup now consists of a container filled with water in which a smaller PVC tube with an inner diameter of 0.65cm is placed. The RPM is placed underneath the container and the ultrasound probe is placed vertically in the water. Figure 5 (A-C) show the ultrasound results of the IRONSperm clusters of samples 2-4 as they are being actuated at a frequency of 0.5Hz and imaged with an ultrasound frequency of 14MHz. The clusters are indicated with white arrows. Figure 5(D) shows the calculated CNR values for increasing concentrations of Fe_3O_4 and it can be seen that for higher concentrations the CNR increases, but for sample 4 it decreases again. Even though the CNR of sample 4 is lower than the CNR of sample 3, the deviation of sample 3 is bigger than that of sample 4. Furthermore, even though the CNR increases up to sample 2, the calculated CNR does not exceed 0.2 however, implying poor image quality. Finally, the cluster sizes of the different samples are not the same, which might also influence the calculated CNR.

IV. Discussion

In order to investigate the influence of Fe_3O_4 nanoparticle concentration on the actuation and localization of IRONSperm clusters, samples with different concentrations of Fe_3O_4 were actuated with an RPM at increasing frequencies until their step-out frequencies were reached. Their average angular velocity was determined at every frequency, which can be related to the magnetic torque exerted on IRONSperm clusters by the RPM.

From Figure 4(D-F) it can be seen that for higher Fe_3O_4 concentrations the average angular velocity is higher than for lower concentrations, which is in accordance with the predictions made based on Equation (2). Despite an increasing angular velocity for higher actuation frequencies, however certain frequencies deviate from this trend. For sample 2 this is the case for frequencies 1.5-3Hz, which are significantly lower than the expected angular velocity of the RPM. For sample 3 there are deviating angular velocities at frequencies 9.5Hz and 10Hz and for sample 4 there are deviating angular velocities at frequencies 6.5Hz and 7Hz, as well as for frequencies 7.5Hz and 8Hz. For sample 4 the decrease in angular velocities at frequencies 6.5Hz and 7Hz, followed by an increase in angular velocity for frequencies 7.5Hz and 8Hz, which seems to coincide with the expected angular velocity of the RPM, all take place above the step-out frequency. This might explain the deviations, since it has been found that, for frequencies above the step-out frequency, the angular velocity of rotating magnetic microrobots is unpredictable [3], [15]. The deviations for samples 2 and 3 take place below the step-out frequency however, and therefore cannot be explained in the same way as sample 4, as it was expected that the angular velocity of samples 2 and 3 would increase up till the step-out frequency and would follow the angular velocity of the RPM. A possible explanation for the deviations of samples 2 and 3 could be that their angular velocities were determined manually using the MATLAB script in Appendix B. This was done by counting the complete number of rotations of the cluster per frequency and dividing the total angular change by the time. For higher frequencies, it was more difficult to accurately determine the total number of rotations however, which might have resulted in inaccurate measurements for the above-mentioned frequencies. To tackle these inaccuracies, all videos were evaluated multiple times and the average number of rotations was calculated, as well as the deviation from the determined average. For future research, it would be better to use a camera with a higher resolution and frame rate, to more accurately determine the angular velocity. Motion tracking might also be used rather than manually counting the number of rotations to minimize the error.

Furthermore, it can be seen that the angular velocities of samples 3 and 4 approximately match the angular velocity of the RPM up till the determined step-out frequencies. This is in accordance with results found in other literature, where the angular velocity below the step-out frequency should match the angular velocity of the RPM [3], [15]. For sample 2 the angular velocity of the cluster only matches that of the RPM for the determined step-out frequency, however. As discussed before, this might also be a result of inaccurate measurements.

From Equation (1) it follows that the magnitude of the magnetic torque of a cluster was dependent on the volume of the cluster, as well as its orientation. During the experimental determination, however the clusters of the different samples varied in size. Because sample 3 existed of smaller clusters, it was impossible to determine the step-out frequency, since it did not fall apart at certain frequencies and performed a uniform rolling locomotion for every frequency. Because no step-out frequency could be determined, sample 3 could not properly be compared to the other samples since the angular velocities at the step-out frequency of each sample were compared to each other. Also because the clusters varied in size, it is not possible to conclude that the higher angular velocities are solely caused by an increase in Fe_3O_4 concentration. Therefore, in future research, when determining the relationship between an increase in Fe_3O_4 concentration and the angular velocity, clusters of the same size have to be used.

Besides investigating the influence of Fe_3O_4 on the actuation of IRONSperm clusters, the influence on the localization using ultrasound was also investigated. In order to investigate the influence on localization, the CNR of ultrasound images was determined. From Figure 5(D). It can be seen that for higher Fe_3O_4 concentrations the CNR also

increases, which is in accordance with the results found in other literature, where an increase in Fe_3O_4 resulted in higher CNR values [17]. In their research, Yang *et al.* did however find that after a certain concentration of Fe_3O_4 nanoparticles, the brightness would decrease. The concentration for which the brightness would decrease was, however, around 90μg/ml, whereas in this research, samples with a concentration in the order of mg/ml were used. For sample 4, the calculated CNR decreases compared to sample 3, however, since sample 3 has a larger deviation in CNR values compared to sample 4, it is expected that this decrease is rather due to inaccuracies in the CNR calculation than a threshold concentration that was crossed. A possible explanation for the large deviation in CNR values for samples 2 and 3 is that the CNR was calculated using the MATLAB script in Appendix C, in which the ROI and background region had to be drawn manually for each second in the ultrasound video. Because of the manual determination of the ROI and background, the CNR calculation is prone to errors, which were tackled by evaluating each video multiple times and calculating the mean CNR and deviation from the mean. Furthermore, despite an increase in CNR, the calculated CNR did not exceed 0.2, which corresponds to poor image quality. Also, because the cluster size varied, it cannot be concluded that the increase in CNR is solely due to an increase in Fe_3O_4, since cluster size may also have an influence. Therefore, it is suggested that for future research, the CNR must be determined by different clusters of approximately the same size.

Before investigating the influence of Fe_3O_4 concentration on the actuation of IRONSperm clusters, predictions were made for the magnetic torque exerted on the cluster by the external magnetic field created by the RPM. In order to make this prediction, the IRONSperm cluster was considered to be a soft magnetic, ellipsoidal body. In reality, however, a cluster of IRONSperm is not truly a soft magnetic, ellipsoidal body. This is because only the Fe_3O_4 can be considered to be soft magnetic. The bovine sperm cells are not magnetic and a cluster of IRONSperm thus does not truly satisfy the approximation of a soft magnetic body. A cluster of IRONSperm is also not perfectly ellipsoidal as can be seen in Figure 4(A-C).

Besides a magnetic torque, the IRONSperm cluster will also likely undergo a viscous drag torque and a friction torque. There would be a drag torque because a cluster of IRONSperm is in reality porous and permeable and when it rolls through a fluid it then experiences a drag torque [3], [19]. There would also be a friction torque because the cluster is rolling along a surface and the contact between these two causes friction. This drag and friction torque will work in the opposite direction of the magnetic torque. To get a more accurate prediction of the rolling motion of a cluster, rather than just the magnetic torque, all these torques would have to be included in future research.

Furthermore, the CNR of different IRONSperm samples was determined at a frequency of 0.5Hz. Ideally, it would be best to determine the CNR of IRONSperm clusters at their determined step-out frequency because at the step-out frequency, the clusters reach their maximum angular velocity, which is most desired for *in vivo* applications since it is the fastest. The step-out frequency is, however, dependent on cluster geometry and because the actuation and localization measurements were performed during different tests, the cluster geometry differed for both tests, even though the same amount of IRONSperm was used. This means that the step-out frequency of the clusters for both tests differed and first had to be determined again to actuate the clusters at the step-out frequency during the localization testing. Therefore, in future research, it is necessary to perform the actuation and localization tests at the same time, to avoid changes in cluster geometry. This change in cluster geometry also poses a problem for *in vivo* applications, because it is likely that for each use, the geometry will have changed. Therefore a better understanding of cluster formation is required, in order to tackle the problem of changing cluster geometry.

The biocompatibility of IRONSperm clusters with different concentrations of Fe_3O_4 has not been investigated in this research. It was however expected that with an increasing concentration of Fe_3O_4, the biocompatibility would decrease, based on previous research. In their research, Gong *et al.* found excellent biocompatibility via incubation of HeLa cells, whereas Middelhoek *et al.* found a slightly reduced viability of HeLa cells of 80%. Yan *et al.* also found reduced viability just above 80% when tested on a fibroblast cell line but drastically reduced viabilities when tested on two cancer cell lines [2]–[4], [7]. If the biocompatibility would indeed decrease, the optimal concentration of Fe_3O_4 would be determined by divining a biocompatibility threshold for which the samples would still be considered biocompatible. This threshold can be determined based on ISO10993-5, which describes test methods to assess the *in vitro* cytotoxicity of medical devices [20]. The samples that achieved the highest angular velocities and ultrasound CNR, but still stayed within the limits of a biocompatible microrobot, would then be considered to be the most optimal. Because the biocompatibility was not tested, however, no threshold could be established. This means that the optimal concentration would be achieved for the sample that achieved the highest angular velocities and ultrasound CNR. For future *in vivo* applications, it is, however, necessary to investigate the biocompatibility of IRONSperm clusters so as to not cause any harm to the human body during *in vivo* applications.

V. Conclusion

The concentration of Fe_3O_4 attached to the surface of IRONSperm cells influences their actuation and localization. We have shown that for increasing concentrations of Fe_3O_4 the step-out frequency, as well as their average angular velocity at this step-out frequency increases. Because the cluster size of the different samples also varied however, this increase in step-out frequency and angular velocity cannot be concluded to be the result of an increase in Fe_3O_4 concentration only. We have also shown that for an increase in Fe_3O_4 concentration, the CNR of ultrasound images increases, but did not exceed 0.2. Once again however, the cluster size was not constant and therefore the increase in CNR cannot be concluded to be the result of an increase in Fe_3O_4 concentration only. In future research, the influence of Fe_3O_4 concentration on the actuation and localization of IRONSperm would have to be investigated

for different clusters with equal sizes. Furthermore, the biocompatibility of IRONSperm clusters with different concentrations of Fe_3O_4 has to be investigated because the biocompatibility is the limiting factor in determining the optimal Fe_3O_4 concentration. Determining the influence of Fe_3O_4 will help in deciding which consistency can best be used to optimize the actuation and localization of IRONSperm in future research, while not exceeding biocompatibility thresholds. This is essential for further developments towards *in vivo* applications.

APPENDIX A

```
% Define parameters
m_0 = (4*pi)*10^-7;
B = 10^-3;
H = B/m_0;

% Calculate volume of an ellipsoidal body
unique_axis = [5*10^-6: 2*10^-6: 15*10^-6];
other_axes = [2.5*10^-6: 1*10^-6: 7.5*10^-6];
v = 4/3.*pi.*unique_axis.*(other_axes).^2; %
xvol = v.*10^18;

% Define angles of orientation
theta = [0:9:45];
angle = sind(2.*theta);

% Calculate demagnetizing factors
R = unique_axis/other_axes;
n_a = 1./(R.^2-1).*(R./(2*sqrt(R.^2-
1)).*log((R+sqrt(R.^2-1))./(R-sqrt(R.^2-1)))-1);
n_r = (1-n_a)/2;

% Define empty torque matrix
T = zeros(length(v),length(theta));

% Calculate torque for different volumes and angles
for i = 1:length(v)
    for j = 1:length(theta)
        T(i,j) = ((m_0.*v(i).*abs(n_r-
n_a))./(2*n_r.*n_a)).*sind(2.*theta(j)).*H^2;
    end
end

% Define parameters
M = .5*10^6;
K = 13*10^3;

% Calculate volume of one nanoparticles
unique_axis_NP = 10*10^-9;
other_axes_NP = 5*10^-9;
V = 4/3.*pi.*unique_axis_NP.*(other_axes_NP).^2;

% Calculating torque of one nanoparticle
t_max = m_0*M*V*H;
t1 = t_max*sqrt(1-((m_0*M*H)/(2*K))^2);

% Define parameters for calculating number of
nanoparticles in total volume
% of nanoparticles
N = 6.022*10^23;
rho = 5170;
M = 0.231533;
Volnano = [0, 50*10^-6, 100*10^-6 , 150*10^-6];
concentration = [0, 1, 2, 3];

% Calculating number of particles with the volume of
nanoparticles
NO = (N*rho*Volnano)/M;

% Define empty torque matrix
t = zeros(length(Volnano),1);

% Calculate torque on increasinf
for m = 1:length(NO)
        t(m) = t1.*sqrt(NO(m));
end

% Plotting the results
figure(1)
subplot(1,2,1)
hold on
for k = 1:length(T)
    plot(T(:,k),'-o');
end
hold off

% Makeup of the figure
lgd =
legend({num2str(theta(1)),num2str(theta(2)),num2str(
theta(3)),num2str(theta(4)),num2str(theta(5)),num2st
r(theta(6))},'location','northwest');
lgd.Title.String= '\theta';
title('Magnetic torque of IRONSperm clusters',
'FontSize', 18);
ylabel('Magitude of torque','FontSize',16);
xlabel('Volume [\mum^3]','FontSize',16);
xticks(1:length(xvol));
xticklabels(num2str(xvol'));
xtickangle(45);
set(gca, 'FontSize', 14);

% Plot results
subplot(1,2,2)
plot(t,'-o');
title('Magnetic torque of nanoparticles',
'FontSize',18);
xlabel('Concentration [mg/ml]', 'FontSize', 16);
ylabel('Magnitude of torque', 'FontSize', 16);
xticks(1:length(concentration));
xticklabels(num2str(concentration'));
set(gca, 'FontSize', 14)
```

APPENDIX B

```
%% Calculate angular velocity for different samples
% Choose video file
[name,path] = uigetfile('*.mp4');
File = fullfile(path, name);

% Read video file
Reader = VideoReader(File);

% Input frame number at which a complete number of
rotations is completed
frameNumber = input('Frame: ');

% Define time that corresponds to the chosen frame
Reader.CurrentTime = frameNumber / Reader.FrameRate;
disp(['Current time: ',
num2str(Reader.CurrentTime)]);

% Calculate average angular velocity
numRotation = input('Number of complete rotations:
');
angularVelocity = (360 * numRotation) /
Reader.CurrentTime;
angularVelocityRad = angularVelocity * (pi/180);
disp(['Average Angular Velocity:
',num2str(angularVelocityRad),' Rad/s']);

%% Plot results
% Gather data from angular velocity calculations
frequency = 0:0.5:12;
w150 =
[0,mean([2.95,2.92,2.89]),mean([6.4,6.33,6.26]),mean
```

```
([9.17,8.98,8.98]),mean([12.64,12.46,12.29]),mean([15.66,15.4,15.15]),mean([17.98,17.69,19.69]),mean([20.94,20.43,20.43]),mean([26.18,24.48]),mean([28.49,27.69,27.69]),mean([31.13,29.76,29.76]),mean([35.90,34.27,34.27]),mean([38.04,36.38,36.38]),mean([17.62,16.83,16.83]),mean([23.32,22.18,22.18]),mean([46.59,44.12,44.12]),mean([49.50,47.12,47.12]),mean([25.70,24.59,24.59]),mean([0]),mean([27.19,25.94,25.94]),mean([12.11,11.57,11.57]),mean([20.02,19.17,19.17]),0,0,0];
errors150 = [0,(2.95-2.89),(6.4-6.26),(9.17-8.98),(12.64-12.29),(15.66-15.15),(17.98-17.69),(20.94-20.43),(26.18-24.48),(28.49-27.69),(31.13-29.76),(35.9-34.27),(38.04-36.38),(17.62-16.83),(23.32-22.18),(46.59-44.12),(49.5-47.12),(25.70-24.59),0,(27.19-25.94),(12.11-11.57),(20.02-19.17),0,0,0];

w100 =
[0,mean([3.11,3.08]),mean([6.24,6.12]),mean([9.42,9.15]),mean([12.88,11.64]),mean([16.25,15.45]),mean([20.49,19.23]),mean([21.92,20.49]),mean([26.18,24.17]),mean([28.56,27.32]),mean([32.5,30.9]),mean([34.27,32.5]),mean([39.27,36.96]),mean([43.98,39.98]),mean([47.12,43.84]),mean([50.94,47.12]),mean([53.86,49.6]),mean([57.12,52.36]),mean([59.77,55.69]),mean([53.86,49.6]),mean([52.36,48.33]),mean([70.01,64.49]),0,0,0];
errors100 = [0,(3.11-3.08),(6.24-6.12),(9.42-9.15),(12.88-11.64),(16.25-15.45),(20.49-19.23),(21.92-20.49),(26.18-24.17),(28.56-27.32),(32.5-30.9),(34.27-32.5),(39.27-36.96),(43.98-39.98),(47.12-43.84),(50.94-47.12),(53.86-49.6),(57.12-52.36),(59.77-55.69),(53.86-49.6),(52.36-48.33),(70.01-64.49),0,0,0];

w50 =
[0,mean([3.47,3.37,3.27]),mean([5.83,5.68,5.54]),mean([5.6,5.51]),mean([6.26,6.13]),mean([7.91,7.77]),mean([9.23,9.11]),mean([21.14,20.20]),mean([10.36,9.82]),mean([13.71,13.11]),mean([12.23,12.67]),mean([8.57,6.98]),mean([3.01,2.93]),mean([2.84,2.77]),mean([2.55,2.49]),mean([3.34,3.28]),mean([1.79,1.75]),mean([6.25,6.11]),mean([3.27,3.16]),mean([1.04,1.0]),mean([1.18,1.16]),0,mean([1.57,1.51]),mean([1.31,1.29]),mean([4.33,4.28])];
errors50 = [0,(3.47-3.27),(5.83-5.54),(5.6-5.51),(6.26-6.13),(7.91-7.77),(9.23-9.11),(21.14-20.20),(10.36-9.82),(13.71-13.11),(13.23-12.67),(8.57-6.98),(3.01-2.93),(2.84-2.77),(2.55-2.49),(3.34-3.28),(1.79-1.75),(6.25-6.11),(3.27-3.16),(1.04-1),(1.18-1.16),0,(1.57-1.51),(1.31-1.29),(4.33--4.28)];

% Calculate angular velocity of the RPM
velocityRPM = frequency .* 2 * pi;

% Plot the results
figure
subplot(1,3,1, 'Position', [0.05, 0.15, 0.29, 0.7]);
hold on
errorbar(frequency, w50, errors50, 'o','MarkerSize',
4,'MarkerFaceColor','b','Color','b');
plot(frequency, w50);
plot(frequency, velocityRPM, 'LineStyle','--',
'Color','g');
hold off

xlabel('Frequency [Hz]','FontSize',14);
ylabel('Angular Velocity [rad/s]','FontSize',14);
ylim([0,25]);
set(gca,'Xtick',(0:1:12));
title('Average Angular Velocity
1mg/ml','FontSize',16);
legend('','Angular velocity cluster','Angular
velocity RPM','Fontsize',14);

subplot(1,3,2, 'Position', [0.37, 0.15, 0.29, 0.7]);
hold on
errorbar(frequency, w100, errors100,
'o','MarkerSize',
4,'MarkerFaceColor','b','Color','b');
plot(frequency, w100);
plot(frequency, velocityRPM, 'LineStyle','--',
'Color','g');
hold off

xlabel('Frequency [Hz]','FontSize',14);
ylabel('Angular Velocity [rad/s]','FontSize',14);
set(gca,'Xtick',(0:1:12));
title('Average Angular Velocity
2mg/ml','FontSize',16);
legend('','Angular velocity cluster','Angular
velocity RPM','Fontsize',14);

subplot(1,3,3, 'Position', [0.69, 0.15, 0.29, 0.7]);
hold on
errorbar(frequency, w150, errors150,
'o','MarkerSize',
4,'MarkerFaceColor','b','Color','b');
plot(frequency, w150);
plot(frequency, velocityRPM, 'LineStyle','--',
'Color','g');
hold off

xlabel('Frequency [Hz]','FontSize',14);
ylabel('Angular Velocity [rad/s]','FontSize',14);
set(gca,'Xtick',(0:1:12));
title('Average Angular Velocity
3mg/ml','FontSize',16);
legend('','Angular velocity cluster','Angular
velocity RPM','Fontsize',14);
```

APPENDIX C

```
%% Calculate CNR for different samples
% Choose video file
[name, path] = uigetfile('*.avi');
File = fullfile(path, name);

% Read video file
Reader = VideoReader(File);
frameRate = Reader.FrameRate;

% Get the amount of frames per second
framesPerSecond = round(frameRate);

% Initialize variables
numFrames = Reader.NumFrames;
cnrValues =
zeros(1,ceil(numFrames/framesPerSecond));

% Calculate CNR for every second in the vidoe
for i = 1:framesPerSecond:numFrames
    % Read current frame and draw ROI
    frame = read(Reader,i);
    gray = im2gray(frame);
    imshow(gray);
    roi = roipoly(gray);
    background = roipoly(gray) - roi;

    % Apply the ROI mask to the frame
    roiFrame = gray .* uint8(roi);
    backgroundFrame = gray .* uint8(background);

    % Calcualte mean and std of the ROI
    roiMean = mean(roiFrame);
    backgroundMean = mean(backgroundFrame);
```

```
    backgroundStd = std(double(backgroundFrame));

    % Calculate the CNR
    cnr = abs(roiMean - backgroundMean) /
backgroundStd;
    cnrValues(ceil(i/framesPerSecond)) = cnr;
end

% Calculate the average CNR
averageCNR = mean(cnrValues);
disp(['Average CNR : ' num2str(averageCNR)]);

%% Plot CNR results
concentration = [0,1,2,3];
CNR = [0,mean([0.11525, 0.10882, 0.098106]),
mean([0.16461, 0.14657, 0.16086]), mean([0.15207,
0.1468, 0.14833])];
error = [0,(0.11525-0.098106), (0.16461 - 0.14658),
(0.15207 - 0.1468)];

figure()
hold on
errorbar(concentration, CNR, error,
'o','MarkerSize',
4,'MarkerFaceColor','b','Color','b');
plot(concentration, CNR);
hold off

xlabel('Concentration [mg/ml]','FontSize',12);
ylabel('CNR','FontSize',12);
title('CNR values of different
samples','FontSize',14)
set(gca,'Xtick',(0:1:3));
```

REFERENCES

[1] D. Liu *et al.*, "Biohybrid Magnetic Microrobots for Tumor Assassination and Active Tissue Regeneration," *ACS Appl Bio Mater*, vol. 5, no. 12, pp. 5933–5942, Dec. 2022, doi: 10.1021/ACSABM.2C00880/ASSET/IMAGES/LARGE/MT2C00880_0006.JPEG.

[2] D. Gong, N. Celi, D. Zhang, and J. Cai, "Magnetic Biohybrid Microrobot Multimers Based on Chlorella Cells for Enhanced Targeted Drug Delivery," *ACS Appl Mater Interfaces*, vol. 14, no. 5, pp. 6320–6330, Feb. 2022, doi: 10.1021/ACSAMI.1C16859.

[3] K. I. N. A. Middelhoek, V. Magdanz, L. Abelmann, and I. S. M. Khalil, "Drug-Loaded IRONSperm clusters: modeling, wireless actuation, and ultrasound imaging," *Biomedical Materials*, vol. 17, no. 6, p. 065001, Sep. 2022, doi: 10.1088/1748-605X/AC8B4B.

[4] V. Magdanz *et al.*, "IRONSperm: Sperm-Templated soft magnetic microrobots," *Sci Adv*, vol. 6, no. 28, pp. 5855–5863, Jul. 2020, doi: 10.1126/SCIADV.ABA5855/SUPPL_FILE/ABA5855_SM.PDF.

[5] F. Rajabasadi *et al.*, "Multifunctional 4D-Printed Sperm-Hybrid Microcarriers for Assisted Reproduction," *Advanced Materials*, vol. 34, no. 50, p. 2204257, Dec. 2022, doi: 10.1002/ADMA.202204257.

[6] M. Medina-Sánchez, L. Schwarz, A. K. Meyer, F. Hebenstreit, and O. G. Schmidt, "Cellular Cargo Delivery: Toward Assisted Fertilization by Sperm-Carrying Micromotors," *Nano Lett*, vol. 16, no. 1, pp. 555–561, Jan. 2016, doi: 10.1021/ACS.NANOLETT.5B04221/SUPPL_FILE/NL5B04221_SI_007.AVI.

[7] X. Yan *et al.*, "Multifunctional biohybrid magnetite microrobots for imaging-guided therapy," *Sci Robot*, vol. 2, no. 12, Nov. 2017, doi: 10.1126/SCIROBOTICS.AAQ1155/SUPPL_FILE/AAQ1155_SM.PDF.

[8] H. Xie *et al.*, "Reconfigurable magnetic microrobot swarm: Multimode transformation, locomotion, and manipulation," *Sci Robot*, vol. 4, no. 28, Mar. 2019, doi: 10.1126/SCIROBOTICS.AAV8006/SUPPL_FILE/AAV8006_SM.PDF.

[9] S. Pane, V. Iacovacci, E. Sinibaldi, and A. Menciassi, "Real-time imaging and tracking of microrobots in tissues using ultrasound phase analysis," *Appl Phys Lett*, vol. 118, no. 1, Jan. 2021, doi: 10.1063/5.0032969/39902.

[10] B. Wang *et al.*, "Endoscopy-assisted magnetic navigation of biohybrid soft microrobots with rapid endoluminal delivery and imaging," *Sci Robot*, vol. 6, no. 52, p. 2813, Mar. 2021, doi: 10.1126/SCIROBOTICS.ABD2813.

[11] I. S. M. Khalil, A. Fatih Tabak, A. Klingner, and M. Sitti, "Magnetic propulsion of robotic sperms at low-Reynolds number," *Appl Phys Lett*, vol. 109, no. 3, p. 33701, Jul. 2016, doi: 10.1063/1.4958737/1078297.

[12] V. Magdanz *et al.*, "Impact of Segmented Magnetization on the Flagellar Propulsion of Sperm-Templated Microrobots," *Advanced Science*, vol. 8, no. 8, Apr. 2021, doi: 10.1002/ADVS.202004037.

[13] V. Magdanz, J. Gebauer, P. Sharan, S. Eltoukhy, D. Voigt, and J. Simmchen, "CommuniCation Sperm-Particle Interactions and Their Prospects for Charge Mapping," 2019, doi: 10.1002/adbi.201900061.

[14] J. J. Abbott, O. Ergeneman, M. P. Kummer, A. M. Hirt, and B. J. Nelson, "Modeling Magnetic Torque and Force for Controlled Manipulation of Soft-Magnetic Bodies," *IEEE TRANSACTIONS ON ROBOTICS*, vol. 23, no. 6, 2007, doi: 10.1109/TRO.2007.910775.

[15] A. W. Mahoney, N. D. Nelson, K. E. Peyer, B. J. Nelson, and J. J. Abbott, "Behavior of rotating magnetic microrobots above the step-out frequency with application to control of multi-microrobot systems," *Appl Phys Lett*, vol. 104, no. 14, p. 144101, Apr. 2014, doi: 10.1063/1.4870768/125354.

[16] J. Carrey and N. Hallali, "Torque undergone by assemblies of single-domain magnetic nanoparticles submitted to a rotating magnetic field," *Phys Rev B*, vol. 94, no. 18, p. 184420, Nov. 2016, doi: 10.1103/PHYSREVB.94.184420/FIGURES/15/MEDIUM.

[17] F. Yang, Y. Li, Z. Chen, Y. Zhang, J. Wu, and N. Gu, "Superparamagnetic iron oxide nanoparticle-embedded encapsulated microbubbles as dual contrast agents of magnetic resonance and ultrasound imaging," *Biomaterials*, vol. 30, no. 23–24, pp. 3882–3890, Aug. 2009, doi: 10.1016/J.BIOMATERIALS.2009.03.051.

[18] A. Rodriguez-Molares *et al.*, "The Generalized Contrast-to-Noise Ratio: A Formal Definition for Lesion Detectability," *IEEE Trans Ultrason Ferroelectr Freq Control*, vol. 67, no. 4, pp. 745–759, Apr. 2020, doi: 10.1109/TUFFC.2019.2956855.

[19] Y. Mu, T. T. Ren, and H. Q. Yu, "Drag coefficient of porous and permeable microbial granules," *Environ Sci Technol*, vol. 42, no. 5, pp. 1718–1723, Mar. 2008, doi: 10.1021/ES702708P/ASSET/IMAGES/LARGE/ES-2007-02708P_0008.JPEG.

[20] "ISO 10993-5:2009(en), Biological evaluation of medical devices — Part 5: Tests for in vitro cytotoxicity." https://www.iso.org/obp/ui/en/#iso:std:iso:10993:-5:ed-3:v1:en (accessed Jun. 26, 2023).